IMECE2019-11295

SOOT MASS ESTIMATION FROM ELECTRICAL CAPACITANCE TOMOGRAPHY IMAGING FOR A DIESEL PARTICULATE FILTER

Salah Hassan

Indiana University Purdue University Indianapolis Indianapolis, IN, USA

Sohel Anwar¹

Indiana University Purdue University Indianapolis Indianapolis, IN, USA

ABSTRACT

The Electrical capacitance tomography (ECT) method has recently been adapted to obtain tomographic images of the cross section of a diesel particulate filter (DPF). However, a soot mass estimation algorithm is still needed to translate the ECT image pixel data to obtain soot load in the DPF. In this paper, we propose an estimation method to quantify the soot load in a DPF through an inverse algorithm that uses the ECT images commonly generated by a back-projection algorithm. The grayscale pixel data generated from ECT is used in a matrix equation to estimate the permittivity distribution of the cross section of the DPF. Since these permittivity data has direct correlation with the soot mass present inside the DPF. a permittivity to soot mass distribution relationship is established first. A numerical estimation algorithm is then developed to compute the soot mass accounting for the mass distribution across the cross-section of the DPF as well as the dimension of the DPF along the exhaust flow direction. Experimental data has been used to validate the proposed soot estimation algorithm which compared the estimated values with the actual measured soot mass. The estimated soot mass for various soot load amounts were found to correlate reasonably well with the measured soot masses in those cases.

Keywords: Electrical capacitance tomography, diesel particulate filter, soot load, electrical capacitance tomography, robust design, fuel efficiency.

1. INTRODUCTION

It has been estimated that emission from diesel engines accounts for two-thirds of all particulate matter (PM) from the US transportation sources. Particulate matter or soot is created

during the incomplete combustion of diesel fuel, which contributes to the problem by releasing particulates directly into the air and by emitting nitrogen oxides and sulfur oxides, which transform into "secondary" particulates in the atmosphere [1]. Due to stricter regulatory requirements for diesel engines emissions, there has been significant research and development work to introduce new technological solutions for the diesel aftertreatment systems in order to meet the emission requirements [1][2]. According to U.S. Environmental Protection Agency (EPA), all diesel engine manufacturers are required to meet these regulatory requirements.

Modern Diesel Engines use a diesel particulate filter (DPF) as shown in figure 1 to capture particulate matter emission with efficiency level of more than 90%. With this type of aftertreatment emission elimination system, DPF retains exhaust gas particles by forcing the gas to flow through the filter and then intermittently burn the captured particles through either an active or a passive regeneration process. This process prevents gradual accumulation of trapped particulate matter inside Diesel Particulate Filter. Without the regeneration process, the trapped particles can clog the filter and creates back pressure in the mean exhaust stream of the engine resulting in a loss of engine efficiency. The back pressure of the engine exerts more loads on pistons, produces more emission, results in higher temperature which can lead to DPF structural failure, and increases fuel consumption.

Hence an accurate estimation of soot load is needed in order to establish the optimal operation of the DPF regenerative process where injected fuel timing plays a major role. This would have positive impact on the DPF life span.

¹ Contact author: soanwar@iupui.edu

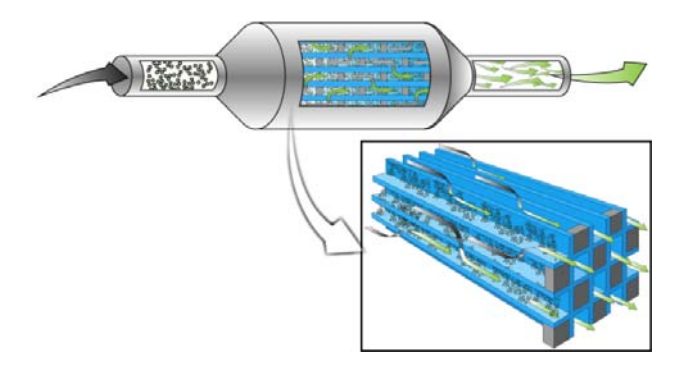


Figure 1: Schematic of a Diesel Particulate Filter [3].

Traditionally estimation of the accumulated soot load inside DPF largely relied on a differential pressure measurement. However, this method has a major drawback with relatively poor accuracy of soot estimation (±50% from the true soot load) [3], specifically at a lower exhaust volumetric flows, and due to the pulsating airflow of engine exhaust gas, which lead to significant irregularities in determining the soot load. Such inaccuracies has direct effect on the efficiency of the regeneration process to purge the restrictive soot load. Since it depends on diesel fuel injection, this affects the optimum operation of the active regeneration process. It has been shown that fuel penalty caused by regeneration could be in the range of (2.2% to 5.3 %) which is more than fuel penalty due to backpressure (1.5% to 2.0 %) [1]. As a result, it is necessary to improve the accuracy of soot load estimation and to accurately determine the regeneration timing.

Electrical capacitance tomography (ECT) has been developed and used since late 1980s for visualization and measurement of a permittivity distribution in a cross section of a pipe carrying fluid using a multi-electrode capacitance sensor [4]. In the past several years there have been a lot of focus on addressing the issue with the measurement of accumulated particular matter inside the DPF, one effective approach is the Electrical Capacitance Tomography using a multi-electrode capacitance sensor to estimate the soot load. This method permittivity utilizes the measurement of the soot load distribution across-section of a DPF using a multi-electrode capacitance sensor. In this paper, a novel approach to estimate DPF's soot load based on its ECT reconstructed image's (pixel) gray-level value is presented. This is done by developing a novel inverse back procejection algorithm that takes into account the proportional relationship between the dielectric soot load filled inside the DPF and the permitivity values calculated using the measured electrical capacitances.

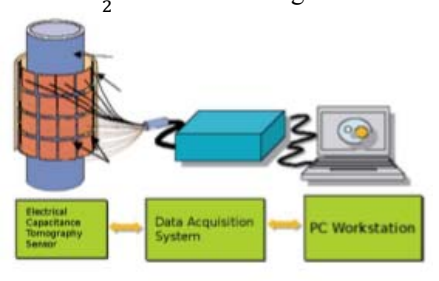
2. ELECTRICAL CAPACITANCE TOMOGRAPHY (ECT) BACKGROUND

Electrical capacitance tomography (ECT) was first introduced in the early 1980s [5]-[7]. It is a method used to determine the spatial permittivity distribution for a region of interest. It is based on the measuring the capacitances between electrodes on the exterior of the region [8].

ECT sensor is widely used in process control for monitoring and control the quality of an industrial process. It is used as one of non-destructive testing methods with potential applications in the measurement of flow of fluids in pipes [9]. It has been adopted in the industry in wide range of applications such as fluid flow monitoring and other industrial applications, however there are some challenges regarding ECT such as low accuracy of its reconstructed images as compared to other methods that are commonly used in image reconstruction [10]. On other hand, capacitive sensors are very convenient because they only consist of electrodes and are sensitive to the electrical properties of materials and their distribution. Moreover, they can work at low frequencies with low power consumption [11].

2.1 ECT Model Design

A basic ECT system normally consists of a capacitance sensor, a measurement unit of capacitance and a computer system for image reconstruction process as shown in figure 2. For a set of n electrodes around the required imaging region, the total number of independent combination of capacitance measurements is $\frac{n(n-1)}{n}$ used for image reconstruction.



3D ECT system diagram and components.

Figure 2: ECT sensor diagram [12].

The sensor is made up of n electrodes mounted on the perimeter of the imaging area. To eliminate external unwanted capacitance known as stray capacitance effects, the electrodes are externally shielded [13]. All independent mutual capacitance measurements are measured between sender electrodes connected to the source signal, and the other receiver electrodes where connected to the ground. Figure 3 shows an ECT sensor with n numbers of electrodes.

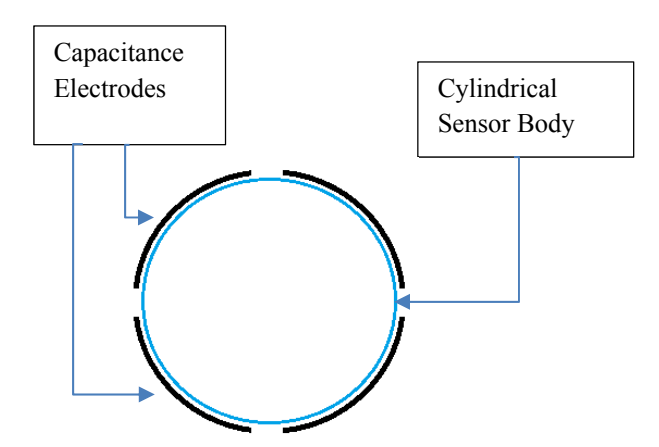


Figure 3: Diagram of a typical ECT sensor.

The capacitance between two pairs of electrodes, i.e. a source electrode and a detector electrode, is obtained through equation (1).

$$Q_i = c_{ii} V_i \tag{1}$$

where Q_i is the charge quantity on electrode i,

 \mathbf{c}_{ij} represents mutual capacitance between electrodes i and j, and V_i is the voltage applied to electrode j.

2.2 Direct Techniques to Generate Sensitivity Matrix

Direct technique is used to generate sensitivity matrix model by measuring the response of capacitance for permittivity perturbations. The basic idea relies on the assumption that the sensitivity is independent of permittivity distribution. The matrix is formed by measuring the capacitances for each a pair of electrodes and constructing array of independent combination of electrodes measurement of high electrical permittivity in the imaging area of interest. Using high and low permittivity material, measurements can be normalized accordingly, as shown in equation (2) [12]:

$$S_i(N) = \frac{C_i(N) - C_i(emp)}{C_i(full) - C_i(emp)}$$
 (2)

where $S_i(N)$ is the sensitivity matrix element [S]

 $C_i(N)$ is the measured capacitance.

 C_i (emp) the capacitance measurement when the sensor is filled with low permittivity.

 C_i (full) the capacitance measurement when the sensor is filled with high permittivity.

2.3 Image Reconstruction using Linear Back Projection

Linear back projection (LBP) was used to process ECT image reconstruction. In LBP, a multidimensional inverse problem needs to be solved. It has the advantage of dynamic and flexible process with good capability of image reconstruction, and it can be expressed as a function of sensitivity matrix as in equation (3) [12]:

$$[C]=[S].[K]$$
 (3)

 $[C] = M_c X 1$ normalized electrode matrix.

To determine the permittivity distribution matrix from the measured capacitance vector, a solution for equation (3) should be obtained.

Let us consider a reconstructed square grid image of N pixels, generated by Linear Back Projection (LBP) algorithm, with known permittivity distribution matrix [S]. From the basic of forward problem algorithm in (3) and the inverse transform Q in (4), an approximation of LBP method uses the transpose of [S] in (3), to have an pseudo-inverse matrix of the dimensions (N x M) that can be used in (5) where [S]^T assumed to be equal to [Q].

$$[K] = [Q]. [C]$$
 (4)

$$[K] = [S]^T . [C]$$
 (5)

[C] = M X 1 matrix containing the normalized electrode-pair capacitances C_M (in the nominal range 0 to 1).

[K] = N X 1 matrix containing the normalized pixel permittivity's (in the nominal range 0 to 1) N is the number of pixels representing the sensor cross-section [1]

[S] = M X N matrix containing the set of sensitivity matrices for each electrode-pair.

3. SIMULATION RESULTS

As the sensitivity matrix forms a basis set from which image vectors can be obtained. Basically, each row of [S] represents the response of the sensor system to a small individual permittivity pixel in a uniform background [13] using direct techniques equation (2) and having normalized capacitance data, a sensitivity matrix has been built.

Table 1: Sensitivity Matrix						
0.000	0.000	0.000	0.000	0.000	0.000	
0.018	0.039	0.058	0.045	0.040	0.044	
0.037	0.078	0.116	0.089	0.079	0.087	
0.203	0.254	0.237	0.134	0.101	0.114	
0.257	0.321	0.251	0.265	0.210	0.197	
0.257	0.315	0.319	0.286	0.283	0.303	
0.257	0.308	0.388	0.307	0.355	0.409	
0.290	0.326	0.419	0.414	0.521	0.452	
0.322	0.343	0.450	0.520	0.686	0.495	
0.487	0.376	0.475	0.611	0.714	0.541	
0.651	0.409	0.500	0.703	0.742	0.587	
0.946	0.579	0.542	0.750	0.752	0.600	
0.953	0.605	0.545	0.753	0.754	0.613	
0.963	0.620	0.559	0.770	0.759	0.614	
0.980	0.681	0.608	0.832	0.813	0.687	
1.000	1.000	1.000	1.000	1.000	1.000	

Table 2: Capacitance (V) measurements for different soot

mass (grams)						
	A-B	A-C	A-D	В-С	B-D	C-D
0	3.63	3.71	3.68	3.75	3.79	3.68
9.35	3.60	3.67	3.61	3.70	3.74	3.64
18.7	3.58	3.62	3.54	3.64	3.69	3.59
37.4	3.34	3.43	3.38	3.59	3.66	3.57
56.3	3.27	3.35	3.37	3.43	3.53	3.49
65.8	3.27	3.36	3.28	3.40	3.44	3.38
84.8	3.27	3.37	3.19	3.37	3.35	3.28
94.2	3.22	3.35	3.15	3.24	3.14	3.24
112	3.17	3.33	3.11	3.11	2.93	3.19
132	2.94	3.29	3.08	3.00	2.90	3.15
151	2.71	3.25	3.05	2.88	2.86	3.10
172	2.30	3.07	3.00	2.82	2.85	3.09
192	2.29	3.04	2.99	2.82	2.85	3.08

210	2.27	3.02	2.98	2.80	2.84	3.08
220	2.25	2.95	2.91	2.72	2.78	3.01
	-	2.60				
FULL						
EMPTY	3.63	3.71	3.68	3.75	3.79	3.68

Once normalized capacitances are obtained [C], a numerical simulation using MATLAB software was used to generate pixel gray-level matrix [K] digital image for all given experimental soot load capacitance measurements. Figures 4, 5, and 6 show the ECT images for soot masses of 172.2, 56.6, and 112.6 grams respectively.

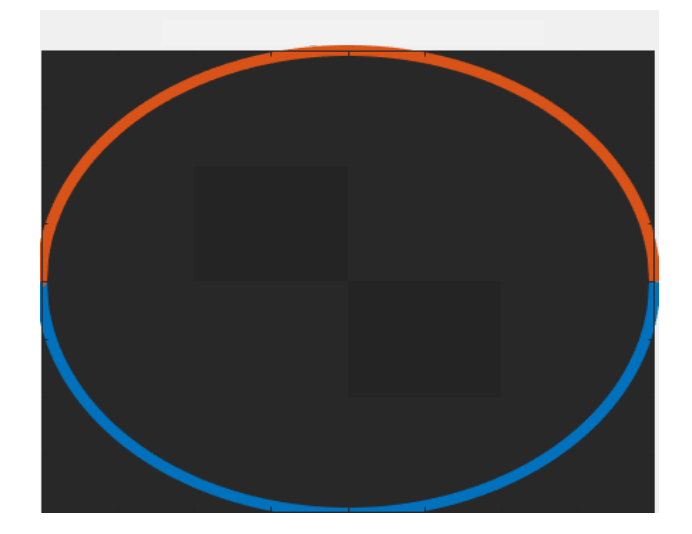


Figure 4: ECT image for a soot mass of 172.2 grams.

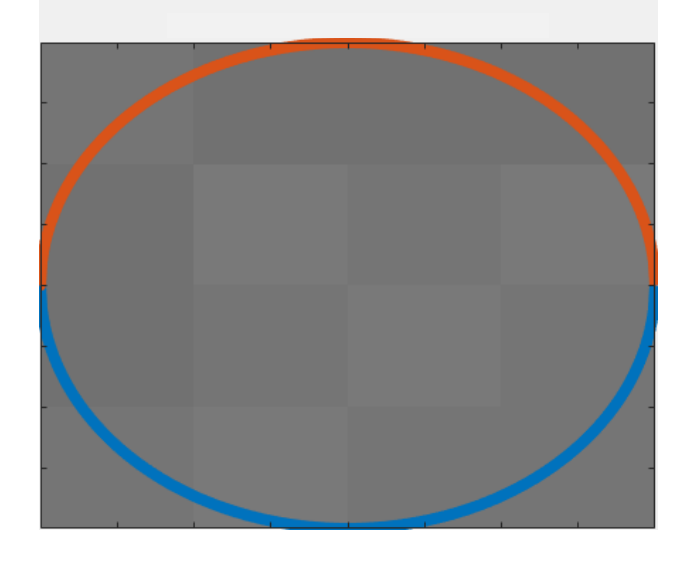


Figure 5: ECT image for a soot mass of 56.6 grams.

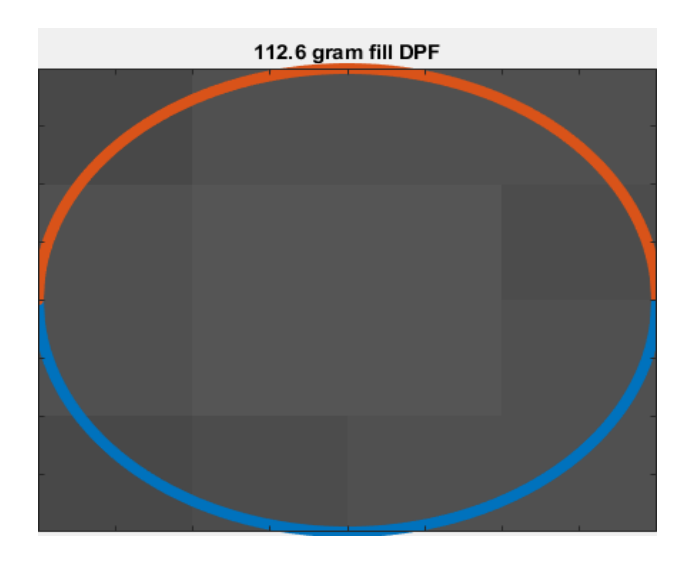


Figure 6: ECT image for a soot mass of 112.6 grams.

4. SOOT MASS ESTIMATION

From the capacitance measurements obtained from inter-electrode data, we can observe the direct relationship between capacitance and material deposited inside the DPF exhibits an inverse relationship. However, the direct contributions of pixels (gray-level) are assumed to be proportional to the actual soot load deposited (W_A) at the time capacitances were measured.

From linear back projection (LBP) algorithm, each of sensitivity matrix multiplied by its corresponding sensor reading to construct the digital image.

It has been observed from the experimental that, change in material deposited (W_{A}) in sensor results in variations in the sensor measured capacitance.

From the experimental data in table 3, a proportional relationship explicitly has been established between sensitivity matrix and actual weight. These results are plotted as shown in figure 7 and represented in polynomial curve from the 6^{th} degree :

$$y = a_1 x^6 + a_2 x^5 + a_3 x^4 + a_4 x^3 + a_5 x^2 + a_6 x + a$$
 (7)

Where \mathbf{y} represents estimated soot mass weight, \mathbf{x} is the gray level value.

Using curve fitting tools in excel a_1 , a_2 , a_3 , a_4 , a_5 , and a_6 can be located respectively as below:

$$a_1 = -1.05$$
E-13 , $a_2 = 1.68761E - 10$ $a_3 = -9.85783E - 08$, $a_4 = 2.5877E - 05$ $a_5 = -0.002829359$, $a_6 = 0.401355946$

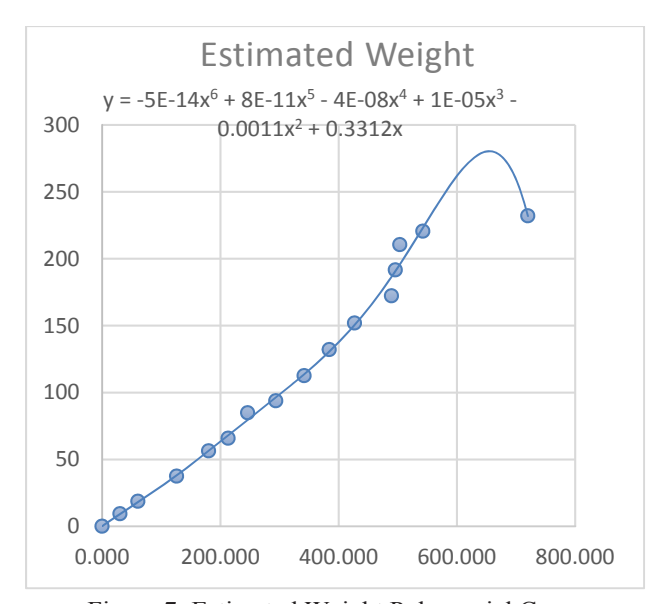


Figure 7: Estimated Weight Polynomial Curve

$$y = -5E-14x^6 + 8E-11x^5 - 4E-08x^4 + 1E-05x^3 - 0.0011x^2 + 0.3312x.$$
 (8)

An estimated weight y can be obtained from the polynomial equation by substituting gray-level value in x at equation right hand as shown in table 3, this direct relationship between gray-level value [K] and actual weight [WA] deposited inside the DPF can be concluded from equation (5),

where
$$C \propto \Sigma K$$
.

An example calculation of the estimated soot weight is shown below. Tables 1-2 show actual weight and sensitivity matrix data, where weight sample of 172.2 gram can be expressed as:

$$[K_{172.2}] = [S]^T$$
. $[C_{172.2}]$

Where

 $[K_{172.2}]$ is gray -level value of 172.2 gram pixel matrix. $[S]^T$ is transpose of Sensitivity Matrix (Table 1). $[C_{172.2}]$ is normalized 172.2 gram victor.

$$[K_{172.2}] =$$

$$\Sigma K_{172.2} = 489.369$$

Substitute Σ K_{172.2} for x in equation (8).

Estimated weight y = 186.35 gram.

The difference between actual and estimated weight (Error) is given by:

Error =
$$(W_E - W_A)/W_A$$

= $(186.35 - 172.2)/172.2$
= 8.22%

Table 3: All estimated weights using nonlinear polynomial equation.

Actual	Gray-Level	Estimated	Error1
Weight	Value	Soot Mass	%
0.00	0.000	0.00	0.00
9.35	30.241	9.18	-1.80
18.70	60.481	17.87	-4.44
37.40	126.032	37.95	1.46
56.30	180.111	56.28	-0.03
65.80	213.169	67.87	3.15
84.80	246.227	79.49	-6.26
93.80	293.962	96.24	2.60
112.60	341.697	113.54	0.83
132.00	384.331	130.55	-1.10
151.90	426.964	150.35	-1.02
172.20	489.369	186.35	8.22
191.60	495.969	190.67	-0.49
210.50	503.527	195.71	-7.03
220.50	542.391	222.93	1.10
232.00	720.000	231.81	-0.08

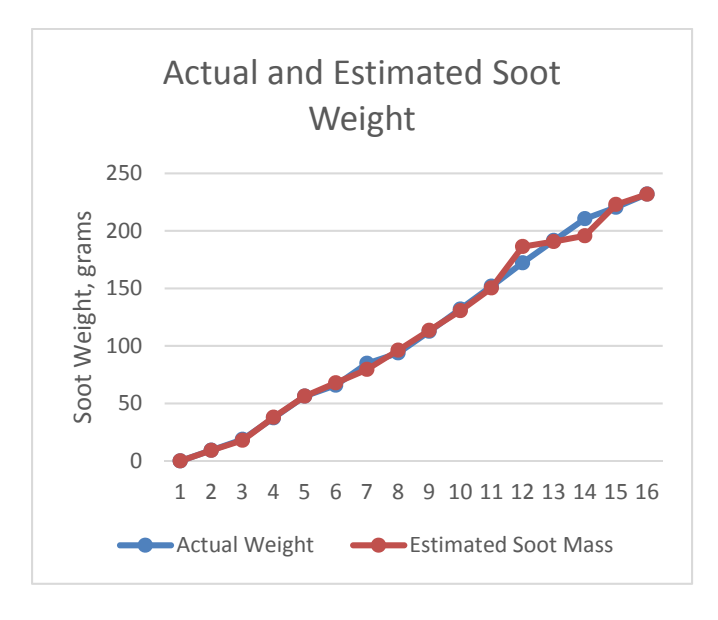


Figure 8: Actual soot mass vs Estimated soot mass.

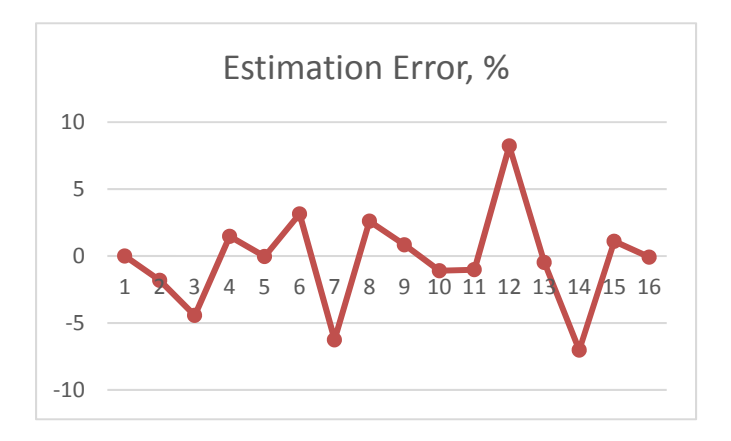


Figure 9: Soot mass estimation accuracy

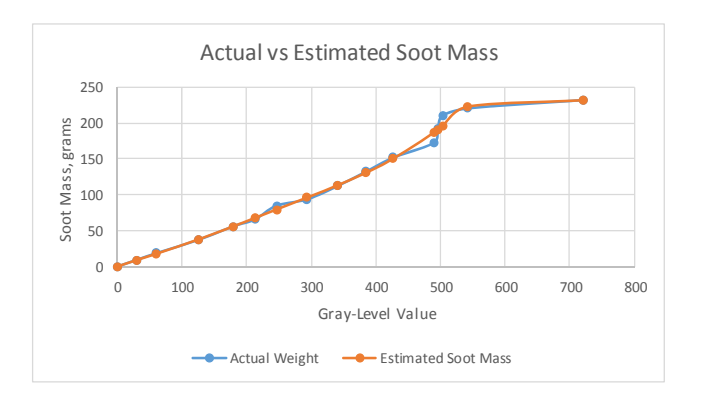


Figure 10: Soot mass comparison with gray level data.

Table 3 shows the estimated soot masses computed using equation (8). It also shows the percentage error based on the actual soot mass for the given tomographic image. Figure 8 shows the estimated vs actual soot masses which is a close match. Figure 9 plots the percentage error for each of the soot mass points. Higher than normal percentage errors was observed at three data points 7th, 12th, and 14th which can be attributed to the low voltage and weight measurement accuracies during the experiment. Estimated soot mass error averages around 5% of the average of the actual soot mass in the DPF for the given tomographic images. Figures 10 show the actual vs. estimated soot mass as a function of the Gray-Level values. This also show a close match between the estimated and actual soot load.

CONCLUSION

The sensitivity matrix for an ECT image forms a basis set from which image pixel data can be obtained via simulation. In this paper, an approach is presented to estimate the soot mass in a Diesel Particulate Filter from an ECT image utilizing its permittivity (capacitance) data. The proposed approach was evaluated for its accuracy against actual soot mass and its corresponding tomographic images. The results obtained by combining the pixel value with soot load physical properties (weight) and permittivity parameters (capacitance) through nonlinear relationship showed reasonable accuracy in estimating the actual soot mass.

REFERENCES

- 1. Huq, Ragibul and Anwar, "Real-time soot measurement in a diesel particulate filter", *US Patent Number 9,151,205*; Issued: October 6, 2015.
- 2. Du, Yanting, Guangdi Hu, Shun Xiang, Ke Zhang, Hongxing Liu, and Feng Guo. "Estimation of the diesel particulate filter soot load based on an equivalent circuit model." *Energies*, vol. 11, no. 2, 2018, pp. 472.
- 3. http://www.drawfolio.com/en/portfolios/ramongarcia-gonzalez/picture/50223#picture-navigation.
- 4. Chen, P. and Wang, J., "Control-oriented model for integrated diesel engine and aftertreatment systems thermal management", *Control Eng. Pract.*, vol. 22, 2014, pp. 81–93.
- Masturah, M. T., M. H. F. Rahiman, Zulkarnay Zakaria, A. R. Rahim, and N. M. Ayob. "Design of Flexible Electrical Capacitance Tomography Sensor." *Jurnal Teknologi*, vol. 77, no. 28, 2015.
- 6. Soleimani, Manuchehr, and William RB Lionheart. "Nonlinear image reconstruction for electrical capacitance tomography using experimental data." *Measurement Science and Technology*, vol. 16, no. 10, 2005, pp 1987–1996.
- 7. White, R., "Using electrical capacitance tomography to monitor gas voids in a packed bed of solids", *Meas. Sci.Technol.*, vol. 13, 2002, pp. 1842–1847.
- 8. Brahma, A., "Modeling and Observability Analysis of DPF Regeneration. In Proceedings of the ASME 2008 Dynamic Systems and Control Conference, Ann Arbor, USA, 20–22 October 2008; pp. 49–55.
- 9. Qussai Marashdeh, "Advances in Electrical Capacitance Tomography", *MS Thesis*, The Ohio State University, 2006, page 24.
- Jaworski, A.J. and Dyakowski, T., "Application of electrical capacitance tomography for measurement of gas-solid flow characteristics in a pneumatic conveying system", Measurement Science and Technology, vol. 12, 2001, pp 1109.
- 11. Huang, S. M., A. B. Plaskowski, C. G. Xie, and M. S. Beck. "Capacitance-based tomographic flow imaging system." *Electronics letters*, vol. 24, no. 7, 1988, pp. 418-419.
- 12. Kowalska, Aleksandra, Robert Banasiak, Radosław Wajman, Andrzej Romanowski, and Dominik Sankowski. "Towards high precision electrical capacitance tomography multilayer sensor structure using 3d modelling and 3d printing method." In 2018 International Interdisciplinary PhD Workshop (IIPhDW), pp. 238-243. IEEE, 2018.
- 13. Marashdeh, Q., and F. L. Teixeira. "Sensitivity matrix calculation for fast 3-D electrical capacitance tomography (ECT) of flow systems." *IEEE transactions on magnetics*, vol. 40, no. 2, 2004, pp. 1204-1207.